Available online at www.sciencedirect.com
ScienceDirect
Trans. Nonferrous Met. Soc. China 33(2023) 3641−3660
Transactions of Nonferrous Metals Society of China
www.tnmsc.cn

Constitutive model for hot deformation behaviors of Al/Cu bimetal composites based on their components

Amir Arsalan SHAYANPOOR, Hamid Reza REZAEI ASHTIANI

School of Mechanical Engineering, Arak University of Technology, Arak, Iran

Received 14 June 2022; accepted 28 October 2022

Abstract: The hot deformation behavior of Al/Cu bimetal composites was investigated using isothermal compression tests at temperatures of 400−500 °C and strain rates of 0.001−0.1 s^{-1} by considering the effects of volume fractions of composite components (30%−51% Al). In this regard, new proper constitutive equations were developed using Arrhenius-type and the rule of mixture (ROM) models. Experimental flow stress (FS) showed that processing parameters and volume fraction affect the flow behavior of composite as the volume fraction of copper has a more substantial impact on the flow behavior of the composite rods at elevated temperatures. The values of correlation coefficient (r) and average relative error of the developed Arrhenius-type constitutive equation and ROM model were 0.9826, 0.9742 and 0.9718, and also 0.18%, 1.69% and −0.84% for volume fractions of 51%, 42% and 30% Al, respectively. The results indicate that the newly developed constitutive model can successfully predict the hot working behavior of the considered bimetal composite. Finally, the microstructure of composites was investigated under different processing conditions. The dominant mechanisms for three considered volume fractions were identified at different temperatures, strains, and strain rates specified for the hot deformation of the Al/Cu composite.

Key words: Al/Cu bimetal composite; hot deformation; rule of mixture (ROM); constitutive equation; mechanical behavior; microstructure

1 Introduction

Today, industries are widely seeking to lighten structures and reduce costs with the development and advancement of science. Recently, the use of bimetallic composite materials has significantly increased in different industries due to obtaining other material properties that cannot be gained from mono-metal samples. Due to the remarkable properties and characteristics of bimetallic composite materials, two or more metal layers, are used in several industries such as automotive, aerospace, electronics, and shipbuilding with advantages such as high conductivity and low conductivity corrosion, and light mass. Al/Cu bimetallic composites are 30%−60% cheaper and lighter than a copper billet [1].

Based on the application, different methods for the production of Al/Cu composites are available such as friction stir welding [2], cold and hot rolling [3,4], various casting methods [5], cold and hot extrusion [1,6], powder reinforced interface layer [7], and explosive welding [8]. SHAYANPOOR and PEZAEI ASHTIANI [7] investigated the microstructure and mechanical properties of the Al/Cu composite at room temperature and identified the intermetallic compounds at the interface between the Al and Cu layers, but the mechanical properties of this composite were not investigated at hot deformation. Also, as one of the necessary processes in the fabrication industry,

Corresponding author: Hamid Reza REZAEI ASHTIANI, Tel: +98-8633400671, Fax: +98-8613670020, E-mail: hr_rezaei@arakut.ac.ir, hrr.Ashtiani@gmail.com

DOI: 10.1016/S1003-6326(23)66360-5

deformation at elevated temperatures is an essential step to control the microstructure and performance of the workpiece, and hot deformation is usually used to increase the properties of the material [9]. Generally, two important parameters are considered for bonding between two metals in the bimetallic composites: the intermetallic phase at the interface and the diffusional condition. In processes performed at room temperature, these interface bonds are usually not formed to achieve a proper interface layer and a heat treatment process and/or fabrication at high temperature should be used for production. Therefore, accurate knowledge of the hot working behavior of Al/Cu composite under various deformation parameters is a prerequisite for industrial production. The behavior of metallic materials at high temperatures is one of the most complex processes that depend on different parameters such as initial grain size, volume fraction of components, phase transformation, secondary phase, forming temperature, and deformation rate.

Simulating the workpiece response under the specified loading conditions requires a proper constitutive equation to model the material behavior in mathematical language. Based on this, the constitutive equation that describes the deformation behaviors of material in the plastic regime is suitable for CAD/CAM software use [10]. For predicting the applied stress to start the plastic regime, under various deformation rates and temperatures, different constitutive equations, consisting of empirical, semi-empirical, physical, phenomenological models, and artificial neural networks have been developed [11−13]. Phenomenological models are developed based on experimental observation using mechanical tests and the Johnson−Cook [14], Khan−Huang−Liang (K-H-L) [15] and Arrhenius-type [16] are examples of phenomenological constitutive models. However, the well-known Arrhenius-type constitutive model with strain compensated model is widely used to model the hot working behavior of other materials such as AA2196 [17], pure copper [18], magnesium alloy [19], titanium [20], and B_4C_p/AA6061 composite [21]. Most applications of constitutive equations are for uniform materials with an investigation on the influence of temperature, strain and strain rate, while for multilayer composites there is a fundamental problem. The main problem is to predict the behavior of hybrid metal composites, the composite must be assumed to be a mono-material, i.e. the effects of each constituent and their volume fraction must be ignored.

In multilayer composites, the relationship between the components and the mechanical behavior of the composite is a very important issue that helps to model the behavior of the composite. Several researchers used the Rule of Mixtures (ROM) for hardness, flow stress (FS), strength, and Young module to examine the volume fraction effect of components [22−24]. FENG et al [25] used the ROM model for Al/Mg composite with a volume fraction of 43%−86% Al to measure the yield strength and flow stress. They reported that ROM's calculated yield strengths have a slight error, but predicted flow curves by the ROM model have a significant difference compared with the experimental results. Although all of these studies are related to the behavior of materials at room temperature, no detailed research has been done to demonstrate the performance of ROM in predicting the behavior of hybrid materials for the hot working process, specifically for Al/Cu bimetal composite.

Given that most studies are based on the fabricated Al/Cu composites, there is no information about the performance of the Al/Cu composite rod under hot working and the effect of different parameters such as volume fraction. Therefore, in this study, the flow behavior of Al/Cu composite rods at elevated temperatures under the hot compression tests was investigated. The effects of processing parameters and volume fraction of components on the plastic FS and corresponding mechanism and microstructure at high deformation temperatures are systematically investigated; after that, the new proper constitutive equations are developed by a combination of Arrhenius-type and ROM models to model the hot FS behavior of the composite based on its components at various strains, temperatures, strain rates, and volume fractions of components.

2 Experimental

2.1 Material

The commercially pure copper (Cu) and AA7022 aluminum alloy were used to fabricate the Al/Cu bimetallic composite, in which Cu alloy is

the sleeve, Al alloy is the core or substrate, and the chemical compositions are listed in Table 1 and Table 2, respectively. In hot deformation, the harder metal becomes softened under annealing to reduce this difference because of a significant difference of FS in aluminum and copper [26]. The copper was heated at 700 °C for 2 h to achieve homogenization and uniform microstructures.

Table 1 Chemical composition of investigated pure copper (wt.%)

Si	Sn	Ag	Al	Fe	Zn	Cu
0.001	0.0147	0.0022	0.0173	0.0183	0.001	99.92

Table 2 Chemical composition of investigated AA7022 alloy (wt.%)

Fe	Ti	Si	Cu	Zn	Mg	Al
0.5	0.1	0.5	0.7	4.8	3.4	Bal.

2.2 Fabrication and extrusion of Al/Cu composite

The sleeve and core with different volume fractions were used to evaluate and compare the strength of the fabricated samples. Hence, to fabricate composite bimetal rods with different volume fractions, copper rods with an outer diameter of 15 mm and different inner diameters (d) of 9, 10 and 11 mm were machined, as shown in Fig. 1. Then, after the drilling and machining process was completed, the surfaces of the parts were washed in acetone solution to remove the handling contaminant and/or oil on the surfaces to achieve a precise fit. The tight-fitting minimizes the air trapped between the two metals, thus preventing from oxidizing of the metals at the interface during hot extrusion. After surface treatment, aluminum billets were symbolized inside the copper cylinder.

After preparing the specimens, extrusion was performed for samples with different volume fractions under isothermal hot extrusion at 500 °C with an extrusion ratio of 1:1.5 and extrusion rate of 4 mm/s. A ceramic furnace with the ability to control the die temperature was used to supply the required heat for the extrusion process. Due to the homogenous temperature distribution of samples and die, samples were heated inside the furnace at the set temperature and kept for 10 min. The hydraulic press with a nominal capacity of 75 t was used for the direct hot-extrusion process and the extrusion force was recorded using a high accuracy load cell (Model: SSMDJM−20kN) with the ability to measure the load force down to 1 kg. The combination of oil and graphite powder was also used as a lubricant among the samples, die, and punch. Due to the difference in thermal expansion between the two metals and the prevention of heat shock to the parts, the hot-extruded Al/Cu composites, leaving the die, were instantaneously quenched in water at 60 ℃. The final diameter of the extruded parts is 12 mm, and other information about assembled parts (initial parts and before forming) is listed in Table 3 and extruded parts (i.e. after forming) as detailed in Table 4. A more detailed description of the manufacturing can be seen in Ref. [7].

2.3 Mechanical properties test

After isothermal hot extrusion, the composite billet samples were prepared for hot compression tests with dimensions of d12 mm × 18 mm, according to the ASTM: E—209 standard, and the schematic of the test design of fabricated composite samples for compression test is shown in Fig. 2. The servo-controlled machine was used to perform

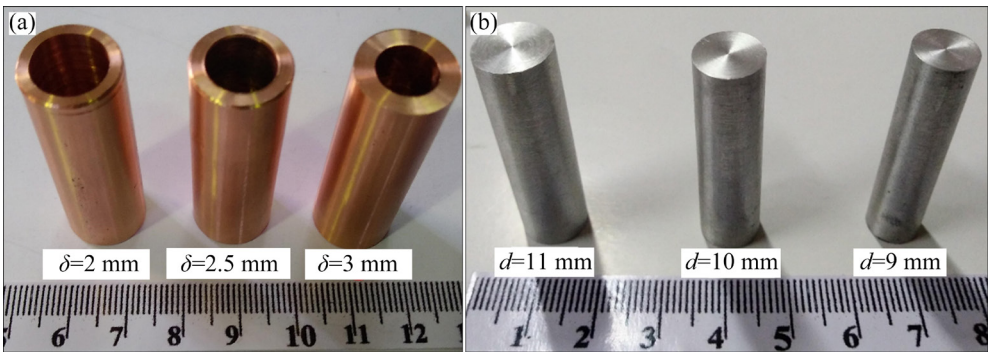

Fig. 1 Sample preparation of copper cylinders (a) and aluminum rods (b) for fabricating Al/Cu bimetal composite with different volume fractions of components (Thickness, δ)

the uniaxial hot compression test up to 60% of total deformation, at temperatures of 400, 450 and 500 °C (i.e. $0.4T_m$ to $0.5T_m$ for copper and $0.61T_m$ to $0.77T_m$ for aluminum) with different strain rates of 0.001, 0.01 and 0.1 s^{-1} to study the true stress−strain of the composite samples. In the present study, the hot compression test was used with the servo-controlled machine (Gotech-AI7000) that is equipped with an electrical resistance furnace and a high accuracy load cell (Model: SSMDJM−20 kN). Due to the homogenous temperature distribution of samples and die, samples were heated at the set temperature and kept inside the furnace for 5 min. In the present study, a thin mica sheet was used to reduce friction between the double face of samples and punched. After hot compression tests, hot deformed samples were immediately quenched in warm water to sustain their microstructure after deformation and prevent the undesirable microstructural alteration.

2.4 Microstructural characterization

The deformed and extruded samples were cut along the compression axis and/or extruded direction with a wire-cut machine for evaluation of the microstructure. Samples were prepared for metallograph with polishing equipment. Due to the difference of chemical corrosion between copper and aluminum, it is challenging to etch the Al/Cu composite samples, and always the main problem in simultaneous etching of Al and Cu is the corrosion and destruction of the diffusion layer between the two metals. Cu was corroded by solution consisting of 67% nitric acid and 33% distilled water, whereas the AA7022 Al alloy was etched by reagent of HF (2 mL) + HNO_3 (5 mL) + HCl (3 mL) + DL water (190 mL) to demonstrate the microstructure of hot extruded and hot compressed samples. Optical microscope and scanning electron microscope (SEM) with energy-dispersive X-ray spectroscopy were used to evaluate the microstructures.

Table 3 Configuration of initial assembled samples

No.	Diameter of Al/mm	Outer diameter of Cu/mm	Inner diameter of Cu/mm	Length of Al/mm	Length of Cu/mm
1	9	15	9	40	42
2	10	15	10	40	42
3	11	15	11	40	42

Table 4 Specification of hot extruded samples

No.	Length of composite/mm	Al reduction/%	Area reduction/%	Thickness of Cu/ mm	Volume fraction/%
1	64	36.3	25	2.7	30
2	64	28.2	25	2.1	42
3	64	27.9	25	1.7	51

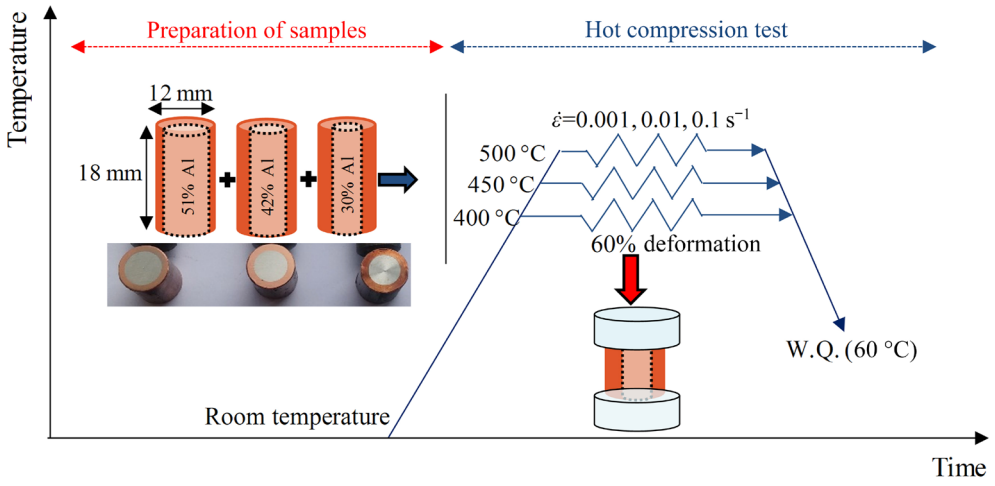

Fig. 2 Compression test schematic of composite samples at various temperatures, strain rates, and volume fractions

The cross-sectional micrographs of Al/Cu composite under different conditions before the hot compression tests or after hot extrusion are shown in Fig. 3. According to Fig. 3, Cu coating is gained by hot extrusion with dense structure and uniform thickness. As is obvious in the SEM images, a good connection is established in samples with various volume fractions of components. The scanning electron microscope with energy-dispersive X-ray spectroscopy (SEM/EDS) and energy spectrum analyses of interface are shown in Fig. 4 which is based on the points specified in Fig. 3. Based on the SEM observation, the interface phase is $CuAl_3$, such a study reported this phase for casting Al/Cu [27] and extruded Al/Cu [28]. These observations show that good conditions are provided for the diffusion of copper and aluminum during the hot extrusion process, which results in the formation of a thin interface layer. These findings are consistent with other copper−aluminum bonding processes under different manufacturing conditions.

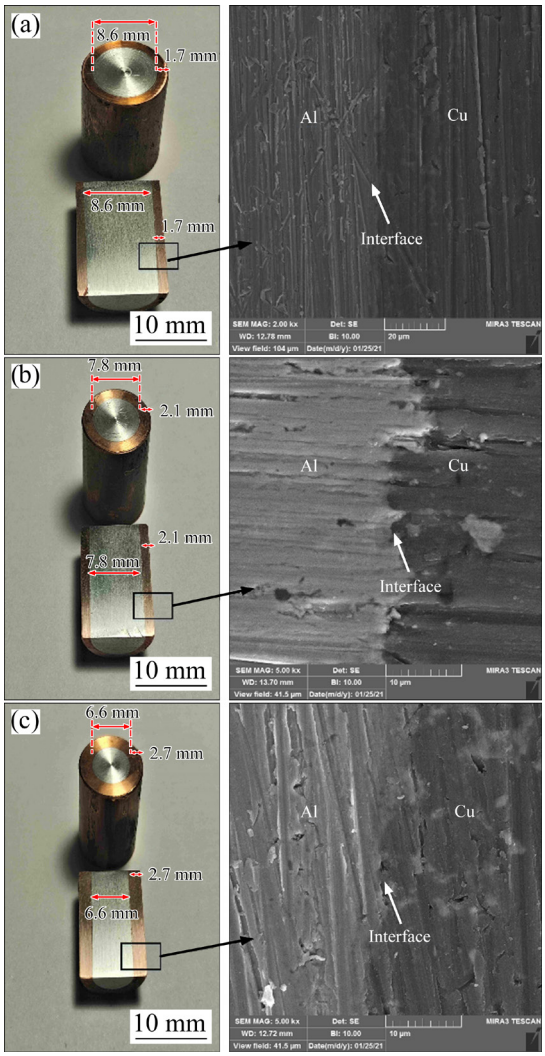

Fig. 3 Micro- and macro-graphs of cross-section of hot extruded Al−Cu composite rods with 51% Al (a), 42% Al (b), and 30% Al (c)

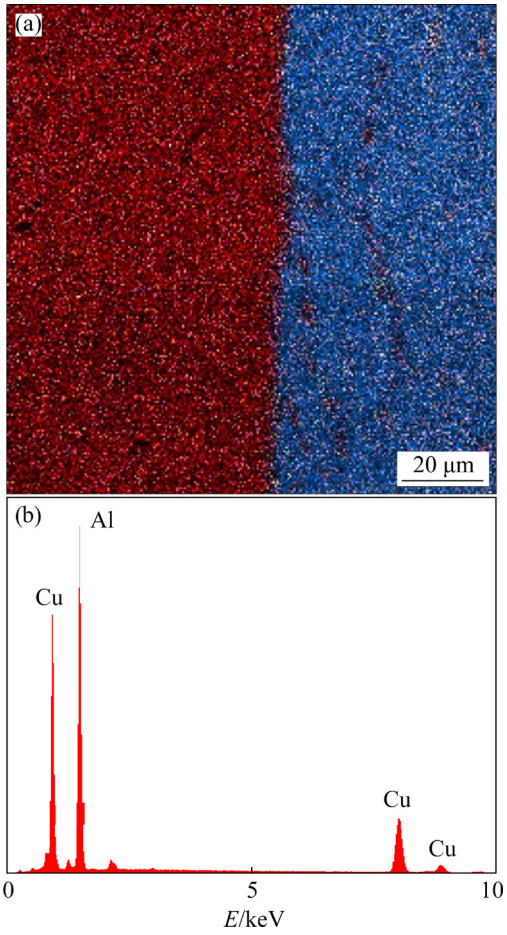

Fig. 4 EDS analysis of Al/Cu interface region: (a) EDS mapping; (b) EDS spectrum

3 Results

3.1 Flow characteristics and deformation mechanisms

The true stress−strain curves of copper-clad aluminum (CCA) rods during the hot compression tests with three volume fractions of components at different strain rates and temperatures are shown in Fig. 5, in which the effect of friction was applied according to Ref. [29]. As shown in Fig. 5, the processing parameters such as temperature, strain rate, and strain have significant effects on the hot flow behavior of the CCA composites. So that the FS of material decreases with increasing temperature from 400 to 500 °C, and the FS of material increases with increasing the strain rate from 0.001

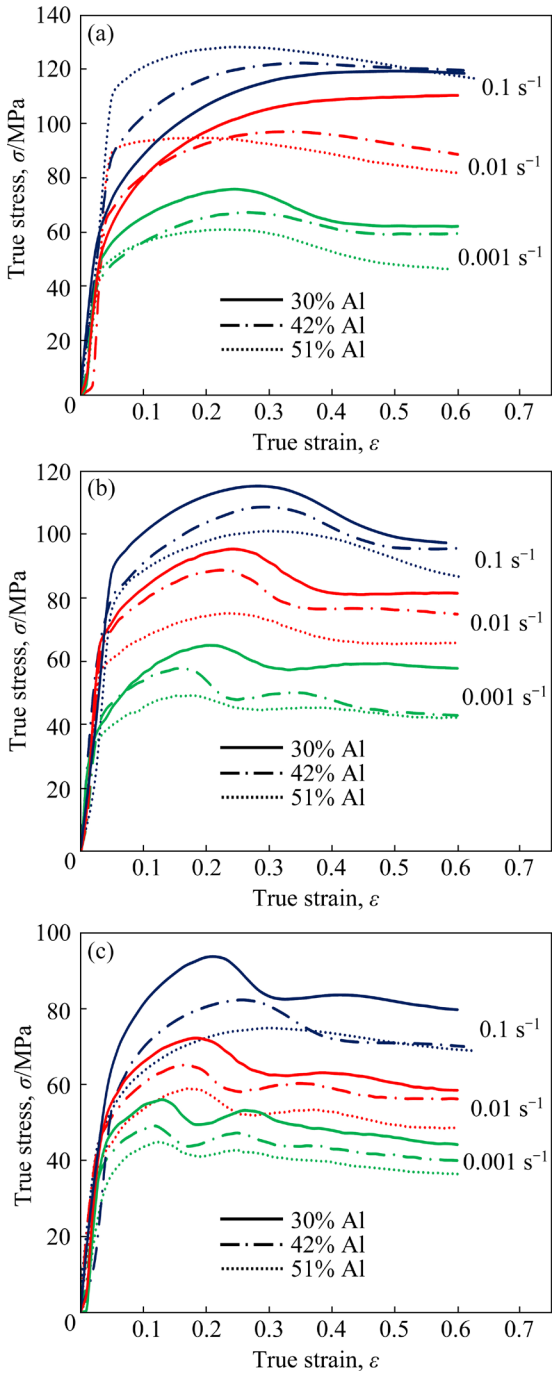

Fig. 5 True stress−strain curves of Al/Cu bimetal composites with strain rates and volume fractions, at deformation temperatures of 400 °C (a), 450 °C (b), and 500 °C (c)

to 0.1 s^{-1}. As can be seen from Figs. 5 and 6, with increasing strain, the FS increases at the initial stage, which indicates the predominance of work hardening and the accumulation of dislocations (Stage I). With increasing strain, the flow stress reaches a steady state after passing the peak value of stress. In other words, the stored energy rapidly increases with increasing strain, which provides a sufficient driving force for the dislocation movement such as dislocation climb or cross-slip. Also, they clearly indicate that thermal softening increases with rising deformation temperature (Stage II). The DRX, DRV, grain growth and annealing twinning are some of the softening mechanisms at the hot deformation of materials [30]. In this regard, annihilation and dislocation reorganization happens to neutralize strain hardening. Finally, due to plastic deformation, the production speed of dislocation becomes equal to annihilation. Therefore, after this process, equilibrium occurs between dynamic softening and works hardening (Stage III). When the deformation rate is high, there is insufficient time and dislocation reaction and recrystallization nucleation will not happen [31]. However, under the relatively high strain rate, the reduction of deformation time restrains the growth of DRXed grains and increases the work hardening effect. The acceleration motion of the dislocation increases, and as a result, the activation energy of thermal diffusion of the CCA increases as the temperature rises [32]. Consequently, the rates of nucleation and recrystallized grain growth rise. So, the FS increases with decreasing temperature and rising strain rate [33,34]. Finally, after the peak value and with increasing strain, the flow stress in some cases decreases and indicates the predominance of the work softening mechanism or the climb and annihilation of the dislocation, and in some cases, a secondary hardening mechanism occurs. The flow softening behavior is probably subjected to dynamic recovery and dynamic recrystallization during hot deformation. Dynamic recovery may occur when the strain rate is higher and/or deformation temperature is lower, at temperature of 400 °C and strain rate of 0.01−0.1 s^{-1}. But dynamic recrystallization takes place with a lower strain rate and higher deformation temperature, which occurs at temperature of 400 °C and strain rate of 0.001 s^{-1} and temperature range of 450−500 °C and strain rates of 0.001−0.1 s^{-1}.

The difference in FS of aluminum and copper is another essential factor in the hot deformation rods and affects the FS diagram is the volume fraction of the composite constituents. The hot deformation of the CCA composite rods is also between the hot deformations of each constituent in each deformation parameter (T, $\dot{\varepsilon}$, ε and V), which

is indicated in Fig. 6 at 500 °C. At elevated temperatures, i.e. at deformation temperatures of $0.4T_m$ to $0.5T_m$ for copper and $0.61T_m$ to $0.77T_m$ for aluminum due to the higher strength of copper than aluminum, the volume fraction of copper has a greater impact on the flow behavior of the composite rods [18,35]. In these conditions, the FS of copper is higher than that of aluminum and the change in the thickness of the sleeve (copper) can more affect the FS. So that the hot working behavior of the composite tends more towards the behavior of aluminum, i.e. the fluctuation of graph or the peak height (due to the softening and hardening mechanism) decreased by increasing the volume fraction of Al. Therefore, it is clear in Fig. 5 that the FS increases with increasing the volume fraction of copper (with increasing the Cu thickness) subsequently with decreasing the volume fraction of Al. Also, according to Fig. 5, the effects of strain rate are reduced with decreasing deformation temperature.

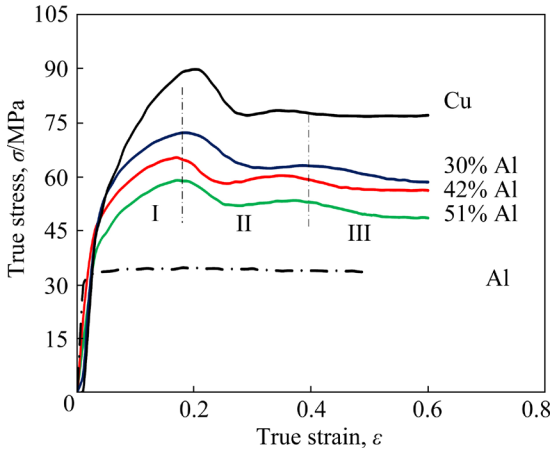

Fig. 6 Effect of volume fraction of CCA composite rods at temperature of 500 °C and strain rate of 0.01 s^{-1}

3.2 Microstructural evolution

The effect of deformation temperature on the microstructures of hot-deformed Al/Cu composites with a volume fraction of 51% Al is shown in Fig. 7. As illustrated, the grain size of microstructure increases with enhancing temperature; some studies have reported these phenomena [18,36]. The accumulation of dislocations and elongated grains occurred in the microstructure at low deformation temperatures while the stored energy in the material increased and more slip systems became active with increasing temperature. Which facilitates the annihilation of dislocation and grain growth [37]. According to Fig. 7(a), elongated grains are perceived in the aluminum structure, and fine-recrystallized grain formation can also be observed around the prior grain boundaries. With increasing temperatures from 400 to 500 °C, the grains grow after the new recrystallization, and the volume fraction of recrystallized grains decreases. Also, the grains grow after the new recrystallization for the copper structure with rising the deformation temperature. It can be explained that DRV quickly consumes energy at low deformation rates. This leads to slow nucleation of the recrystallized grains and it is difficult to keep growing up for recrystallized grains at low temperatures. So, the decomposition of input energy results from thermal diffusion that was not consumed by the changes in microstructure [38].

At low temperatures, the hardening mechanism is the dominant process because thermal activation is not active, which causes to increase the flow stress and indicates that the effect of pinning on dislocation and the characteristic of the high density of dislocation jungle is a symbol of strain hardening at relatively low deformation temperatures [12]. In other words, the hardening stage is accompanied by

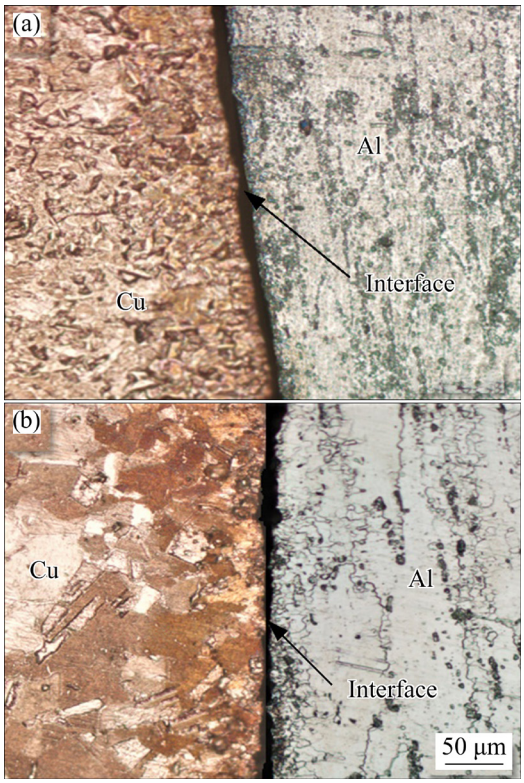

Fig. 7 Microstructures of hot-deformed Al/Cu composite samples with 51% Al under strain rate of 0.001 s^{-1} at 400 °C (a) and 500 °C (b)

the DRV mechanism, and this indicates the formation and accumulation of dislocations [39]. Besides, according to Fig. 7, twinning increases in the copper structure with increasing temperature, and similar results have been reported [40]. This can be explained by the fact that grain growth causes stress to be concentrated at the boundaries where the twins reduce the stress and energy at the boundaries due to the inactive slip system in these areas [41,42], and also grain boundary migration often leads to the formation of twins [42]. As a result, DRV is a dominant mechanism at low deformation temperature, whereas, at high temperature, DRX occurs, and after that, grain growth occurs.

The effect of strain rate on the microstructures of hot-deformed Al/Cu composites with a volume fraction of 30% Al is illustrated in Fig. 8. As can be seen, the grain size of microstructure decreases with increasing deformation rate; some studies have reported these phenomena [43]. This is because there is not enough time to rearrange dislocations and grow recrystallized grains at high strain rates due to lack of sufficient time. As can be seen in Fig. 8(b), some DRX grains near the grain boundary are observed in the microstructures of Al and Cu in hot deformed samples.

The optical metallographs of the hot compressed samples with the volume fractions of 30% and 51% Al are shown in Fig. 9. According to this figure for copper structure, the sample with a volume fraction of 51% Al has a high accumulation of dislocation tangle at the grain boundaries and grains elongate along the compression direction. This microstructural phenomenon is indicative of dynamic recovery (DRV) and it has been shown in the previous study for the hot working behavior of pure copper [18,44]. This can be explained due to the low deformation (reduction) that energy is quickly consumed by DRV. This leads to slow nucleation of the recrystallized grains and it is difficult for recrystallized grains to keep growing up. So, the input energy of deformation is not sufficient, and the thermal energy is decomposed by thermal diffusion where this is not consumed by the changes in microstructure [38]. However, due to the increased copper sleeve reduction with increasing volume fraction of copper, the grains absorb more energy due to more deformation, and fine recrystallized grains form and develop around the

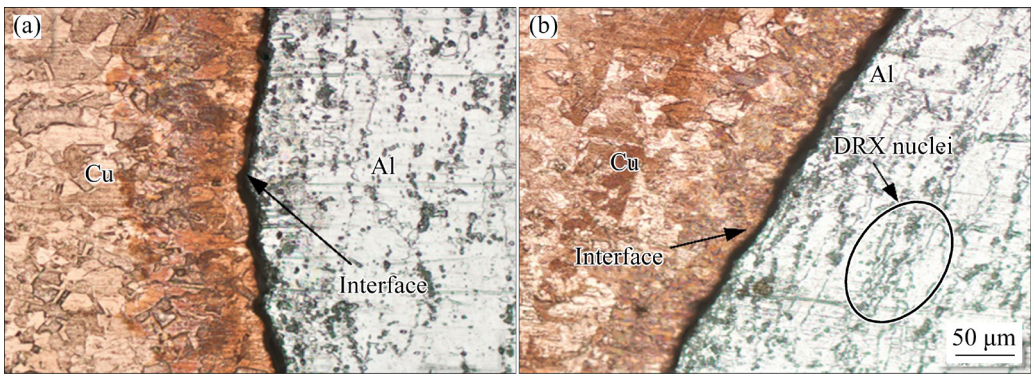

Fig. 8 Microstructures of hot-deformed Al/Cu composite samples with 30% Al at deformation temperature of 450 °C under strain rates of 0.001 s^{-1} (a) and 0.1 s^{-1} (b)

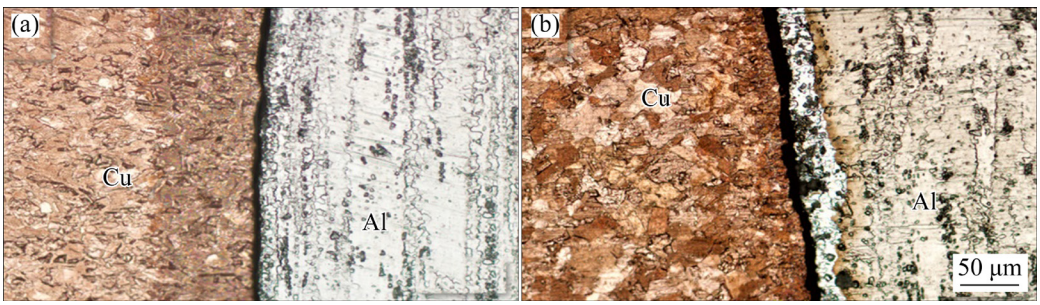

Fig. 9 Microstructures of hot deformed Al/Cu composite samples at strain rate of 0.1 s^{-1} and temperature of 500 °C with volume fractions of 51% Al (a) and 30% Al (b)

prior grain boundaries (Fig. 9(b)). Consequently, the density of the dislocations decreases with increasing Cu reduction, and obviously, the grains become finer and more uniform, suggesting dynamic recrystallization [45]. In three samples, in aluminum, the DRX nucleation occurred at the prior grain boundary and the relatively large non-recrystallized elongated grains are formed in the direction of hot extrusion, this phonon was reported for aluminum alloy after hot extrusion [46]. Consequently, more nucleation of recrystallization occurred on these elements with an increase in the volume fraction of each constituent. In a composite sample with 51% Al (Fig. 9(a)), the aluminum structure has a more volume fraction of recrystallized nucleation compared to the sample with 30% Al (Fig. 8(b)). Also, in the sample with 49% Cu (Fig. 9(a)), the copper structure has a lower volume fraction of recrystallized nucleation than the sample with 70% Cu (Fig. 9(b)).

4 Discussion

4.1 Rule of mixtures in hybrid metal composite

Researchers made many attempts to find the relationship among composites and their constituents to model the strength of a bimetal composite, eventually reaching the ROM, as illustrated in Eq. (1) that applies to composites and sandwich materials [25]:

$$\sigma_C=\sigma_1 V_1+\sigma_2 V_2 \tag{1}$$

where σ_C is the strength of the composite, σ_1 and σ_2 are the strength of components 1 and 2, and V_1 and V_2 are the volume fraction of each component, respectively. The application of the ROM is limited to the thickness of the boundary layer and the dimensions of the structure, so that if the layer thickness and the dimensions are in the nanoscale, the strength of the composite is greater than the predicted strength by the ROM. This is because the density of the interface layer is higher than that in area which is a barrier against the glide of dislocation and increases the strength of the material against deformation. Therefore, by applying more deformation or energy to the system, the response of the material is related to slip, nucleation, annihilation, and rearrangement of dislocations in that area [47]. But researchers have reported that ROMs are well able to predict composite strength for materials with a layer thickness and structure size on a millimeter-scale [23,48].

In this study, Eq. (2) can be written as follows for Al/Cu bimetal composite:

$$\sigma_{CCA}=\sigma_{Al}V_{Al}+\sigma_{Cu}V_{Cu} \tag{2}$$

Therefore, for modeling the hot working behavior of Al/Cu bimetal composites using the rule of mixture needs two parameters of volume fractions (V_{al}, V_{Cu}) and FS of aluminum and copper (σ_{al}, σ_{Cu}). By calculation, the V based on the dimension of manufactured composite needs to specify the FSs of aluminum and copper as constitutive equations. In this investigation, the Arrhenius-type constitutive model was used to predict the hot flow behaviors of aluminum and copper.

4.2 Development of Arrhenius-type constitutive model for Al/Cu composite

A phenomenological equation that can be successfully developed for different materials in different ranges of $\dot{\varepsilon}$ and T is the Arrhenius-type constitutive equation. The Arrhenius constitutive model is usually used to investigate the effect of processing parameters on the FS behavior for optimizing hot working conditions, and generally to predict the FS of metallic materials at elevated temperatures. Therefore, the Zener–Hollomon parameter (Z) is capable of expressing the relation among temperature (T), strain rate ($\dot{\varepsilon}$) and flow stress as follows [12,49]:

$$\begin{cases} Z=\dot{\varepsilon}\exp[Q/(RT)] \\ \dot{\varepsilon}=Af(\sigma)\exp[-Q/(RT)] \end{cases} \tag{3}$$

where

$$f(\sigma)=\begin{cases} \sigma^{n'}, & \alpha\sigma<0.8 \\ \exp(\beta\sigma), & \alpha\sigma>1.2 \\ [\sinh(\alpha\sigma)]^n, & \text{for all } \sigma \end{cases} \tag{4}$$

where $\dot{\varepsilon}$ and σ are strain rate and FS for determining strain, respectively, Q is activation energy on hot deformation (kJ/mol), T is the temperature in K, R is the molar gas constant (8.3144 J/(mol·K)), and n', n, β, A and α ($\alpha=\beta/n'$) are material constants. Generally, for low and high stresses, the power law and the exponential law are suitable and accurate, respectively [10]. In order to obtain the same constancy for the Al/Cu composite, the composite constants can be achieved by

extending each of the extracted coefficients for aluminum and copper using the ROM. The material constants for composites using ROM can be written as follows:

$$\ln A_{CCA}=(\ln A_{Al})V_{Al}+(\ln A_{Cu})V_{Cu} \quad (5)$$

$$Q_{CCA}=Q_{Al}V_{Al}+Q_{Cu}V_{Cu} \quad (6)$$

$$\beta_{CCA}=\beta_{Al}V_{Al}+\beta_{Cu}V_{Cu} \quad (7)$$

$$n_{CCA}=n_{Al}V_{Al}+n_{Cu}V_{Cu} \quad (8)$$

$$\alpha_{CCA}=\alpha_{Al}V_{Al}+\alpha_{Cu}V_{Cu} \quad (9)$$

To calculate the coefficients of the Arrhenius model mentioned above, the true stress−strain data for aluminum and copper obtained from hot compression tests were used, as shown in Fig. 10. The hyperbolic sine Arrhenius coefficients are obtained at a specific strain, which in the current work strain of 0.6 was selected, and the values of FS at this strain are listed in Table 5. In order, by taking the natural logarithm of both sides of Eq. (4), the following equations can be gained for low- and high-stress levels, respectively:

$$\ln \dot{\varepsilon}=n'\ln \sigma+\ln A'-Q/(RT) \quad (10)$$

$$\ln \dot{\varepsilon}=\beta\sigma+\ln A'-Q/(RT) \quad (11)$$

According to Eqs. (10) and (11), there is a linear relationship between stress and strain rate at each temperature, and this relation can be achieved by placing the results of the hot compression tests for two materials in these equations. Then, by taking partial differentiation of Eqs. (10) and (11), the following expressions can be gained, respectively:

$$n'=\left[\frac{\partial \ln \dot{\varepsilon}}{\partial \ln \sigma}\right]_T \quad (12)$$

$$\beta=\left[\frac{\partial \ln \dot{\varepsilon}}{\partial \sigma}\right]_T \quad (13)$$

By using linear regression curve-fitting on lines of $\ln \dot{\varepsilon}-\ln \sigma$ and $\ln \dot{\varepsilon}-\sigma$, the values of n' and β can be obtained at various temperatures, as depicted in Figs. 11(a) and (b) for aluminum and copper, respectively. Therefore, the mean values of β are achieved at 0.1872 and 0.0902 for Al and Cu, respectively, by using the linear curve fitting method of the data points. Also, the mean values of n' were calculated according to Fig. 11(a) for Al and

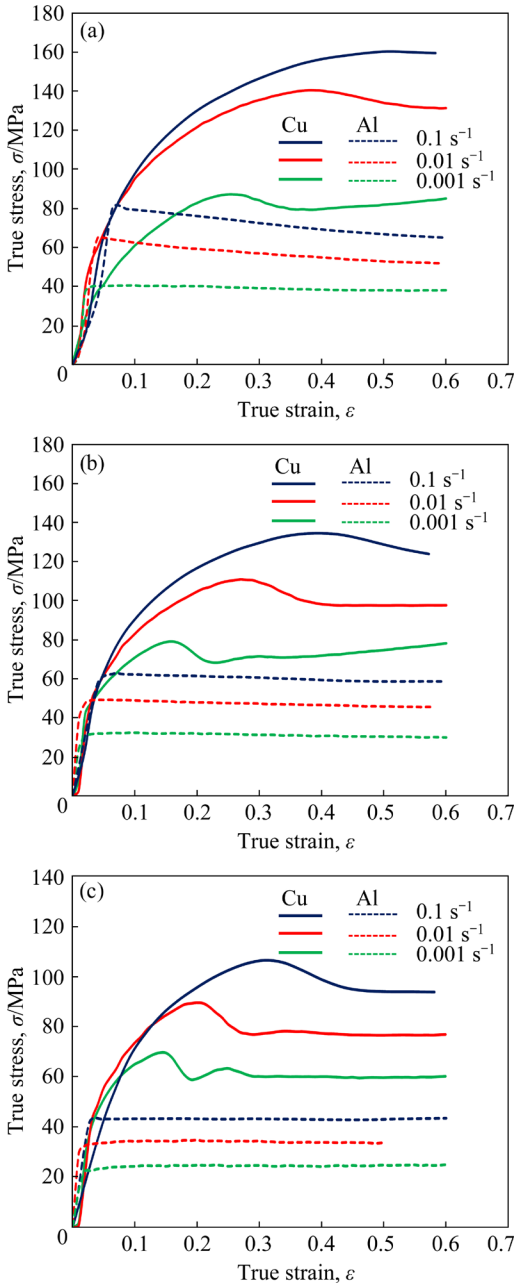

Fig. 10 Flow stress curves of deformed Cu and Al with various processing parameters at deformation temperatures of 400 °C (a), 450 °C (b), and 500 °C (c)

Table 5 Flow stress for Al and Cu at strain of 0.6 under different conditions

Temperature/°C	Flow stress/MPa					
	Al			Cu		
	0.001 s^{-1}	0.01 s^{-1}	0.1 s^{-1}	0.001 s^{-1}	0.01 s^{-1}	0.1 s^{-1}
400	38.07	52.05	65.11	85.18	131.45	159.24
450	29.91	45.55	58.40	78.30	97.52	132.73
500	25.00	33.63	43.25	60.34	77.00	93.92

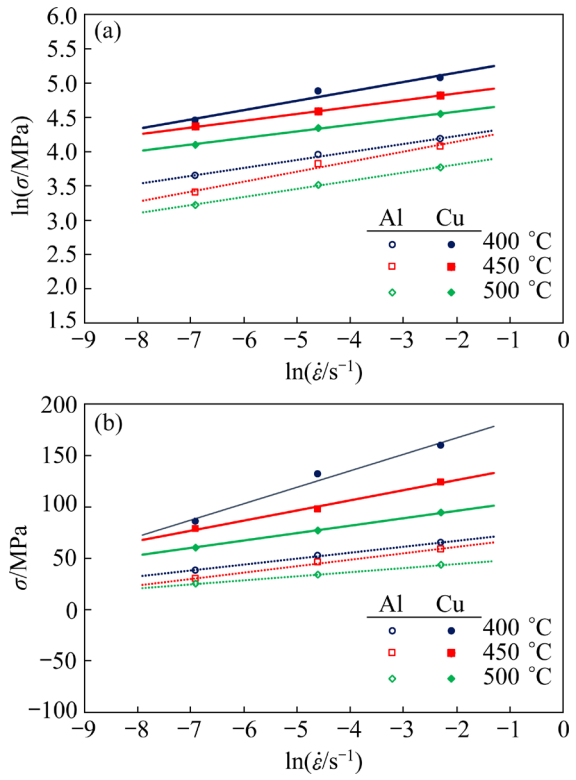

Fig. 11 Relationship plots of $\ln\dot{\varepsilon}-\ln\sigma$ for n' (a) and $\ln\dot{\varepsilon}-\sigma$ for β (b)

Cu at 7.87 and 9.055, respectively. According to Fig. 11(a), the values of n' regularly reductions with rising temperatures. That is because, at low temperatures, diffusion occurs at the grain boundaries (Coble-diffusion flow), but diffusion occurs in the lattice at high temperatures because it needs high energy. The calculated mean value of n' for two materials is higher than the typical value associated with lattice-diffusion controlled dislocation climb (n'=5) [50]. As a result, the mean amount of n' explains the prevalence of diffusion at the grain boundaries. The calculated values of $\alpha=\beta/n'$ are 0.0237 and 0.0099 for aluminum and copper, respectively.

For calculation of Q and n at all levels of stress, the following equation can be written from Eq. (3):

$$\dot{\varepsilon}=A\left[\sinh(\alpha\sigma)\right]^{n}\exp\left(\frac{-Q}{RT}\right) \tag{14}$$

Considering the logarithm of Eq. (14):

$$\ln\dot{\varepsilon}=n\ln\left[\sinh(\alpha\sigma)\right]+\ln A-\frac{Q}{RT} \tag{15}$$

Taking partial derivatives of both sides of Eq. (15):

$$Q=R\left[\frac{\partial\ln\dot{\varepsilon}}{\partial\ln\left[\sinh(\alpha\sigma)\right]}\right]_{T}\left[\frac{\partial\ln\left[\sinh(\alpha\sigma)\right]}{\partial(1/T)}\right]_{\dot{\varepsilon}}=Rn(T)S(\dot{\varepsilon}) \tag{16}$$

According to Eq. (16), there is a linear regression among $\ln\dot{\varepsilon}$ and [sinh($\alpha\sigma$)]. In Eq. (15), n stands for the slope of mentioned lines at a constant temperature, as shown in Fig. 12(a). By separating Eq. (16), Eq. (17) can be obtained:

$$n=\left[\frac{\partial\ln\dot{\varepsilon}}{\partial\ln\left[\sinh(\alpha\sigma)\right]}\right]_{T} \tag{17}$$

At a true strain of 0.6 and each forming temperature, the mean values of n are calculated as 5.94 and 6.83 for aluminum and copper, respectively. Similarly as can be found in Fig. 12(b), the slope of those lines (S) can be acquired by applying linear regression between ln[sinh($\alpha\sigma$)] and ($1/T$) at a constant strain rate. By simplifying Eq. (16), the flowing equation is achieved:

$$Q=Rn(T)\left[\frac{\partial\ln[\sinh(\alpha\sigma)]}{\partial(1/T)}\right]_{\dot{\varepsilon}} \tag{18}$$

Then, by specifying the values of S and n, the values of Q are calculated to be 143 and 185 kJ/mol

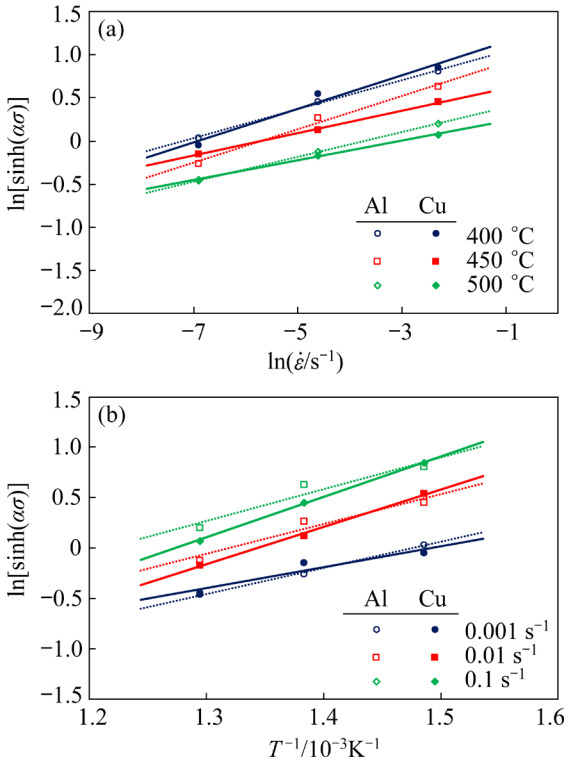

Fig. 12 Relationship plots between $\ln\dot{\varepsilon}$ and [sinh($\alpha\sigma$)] (a) and [sinh($\alpha\sigma$)] and ($1/T$) (b)

for aluminum and copper, respectively. The activation energy explains the complexity of the deformation and/or rate-controlling mechanism. Indeed, Arrhenius's theory states that Q is the energy level that restricts the passage of metal atoms, which is necessary for some atomic mechanisms [51]. The variations of the activation energy map for AA7022 and copper at strain of 0.6 under different temperatures and strain rates are illustrated in Fig. 13. As can be seen, the Q is increased with strain rate and temperature [19,52]. The reason for the increase in Q with the strain rate is due to the accumulation of dislocation. Increasing the strain rate reduces the dynamic restoration time and makes dislocation movement difficult, which causes to increase the accumulation of dislocations and the energy to overcome the obstacles. Also, the values of Q with increasing temperature are more than activation energy (Q_{act}) of self-diffusion of aluminum (142 kJ/mol [53]) and copper (197 kJ/mol [18]), which causes other mechanisms to take place instead of climbing and slipping of dislocation. Consequently, the needed thermal energy increases to overcome the obstacles. The strain effect on activation energy will be investigated in the next section.

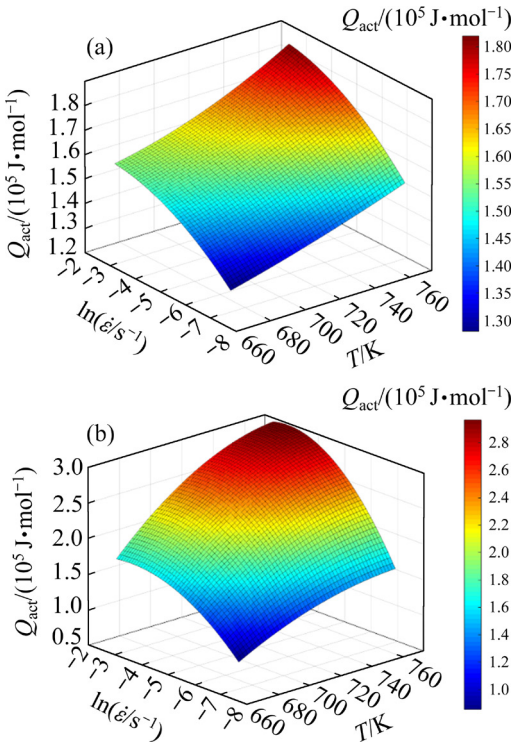

Fig. 13 Variation of activation energy with temperature and strain rate at strain of 0.6 for AA7022 (a) and pure copper (b)

To obtain the final coefficient of the material (A), Eq. (3) for all stress can be rewritten as

$$Z=\dot{\varepsilon}\exp[Q/(RT)]=A[\sinh(\alpha\sigma)]^n \tag{19}$$

After the neutral logarithms are taken from Eq. (19):

$$\ln Z=\ln A+n\ln[\sinh(\alpha\sigma)] \tag{20}$$

Based on Fig. 14, the intercept of plots between ln Z and ln[sin($\alpha\sigma$)] is the value of ln A and can be calculated by linear curve fitting. Eventually, the values of ln A are 18.28 and 25.46 for aluminum and copper, respectively.

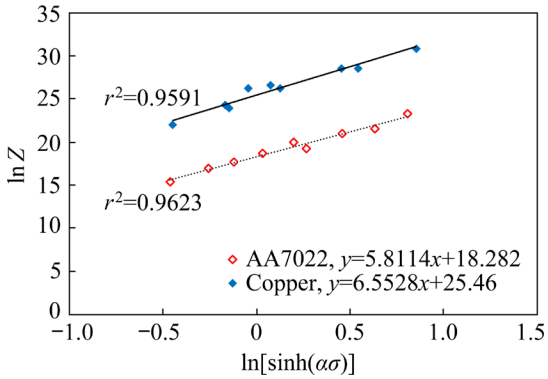

Fig. 14 Relationship between ln$Z$ and ln[sin($\alpha\sigma$)] for copper and AA7022

Finally, after the determination of material constants such as n', n, β, A and α, the developed constitutive equations for hot deformation of AA7022 and pure copper can be represented by the Z parameter as follows.

For AA7022 aluminum alloy:

$$Z=\dot{\varepsilon}\exp\left(\frac{2.40\times10^5}{RT}\right)=1.57\times10^{15}\left[\sinh\left(0.0196\sigma\right)\right]^{5.42} \tag{21}$$

For pure copper:

$$Z=\dot{\varepsilon}\exp\left(\frac{1.85\times10^5}{RT}\right)=1.14\times10^{11}\left[\sinh\left(0.0099\sigma\right)\right]^{6.83} \tag{22}$$

Therefore, by incorporating Eqs. (14) and (19), the flow stress can be predicted using the Z parameter as follows.

For AA7022 aluminum alloy:

$$\sigma=51.02\ln\left\{\left(\frac{Z}{1.57\times10^{15}}\right)^{0.1842}+\right.$$

$$\left[\left(\frac{Z}{1.57\times10^{15}}\right)^{0.3685}+1\right]^{1/2}\Bigg\} \tag{23}$$

For pure copper:

$$\sigma=100.336\ln\left\{\left(\frac{Z}{1.14\times10^{11}}\right)^{0.1463}+\left[\left(\frac{Z}{1.14\times10^{11}}\right)^{0.2927}+1\right]^{1/2}\right\} \tag{24}$$

4.3 Strain-compensated Arrhenius-type constitutive model

The constitutive equations derived above could be models of the hot working behavior of AA7022 alloy and pure copper. But it is important to note that Eqs. (21) to (24) do not consider the effects of strain. On the other hand, in Eqs. (21)−(24), effects of strain rate and temperature are considered. Both the stress−strain curves of the composite constituents and the Al/Cu composite change with strain. Softening mechanisms such as DRX and DRV occur with strain changing; these conditions reveal that strain significantly impacts materials' hot working behavior. Therefore, the strain effects to improve the accuracy of the developed constitutive equation should be considered. So, the material constants of Q, n, β, $\ln A$ and α were determined for various strains, ranging from 0.1 to 0.6 with a step of 0.05, as shown in Eq. (25) [54]. The relationships between material constants and strain for AA7022 alloy and copper are plotted in Fig. 15. As can be found from the figure, the fifth-order polynomial curve fitting functions could provide a good relation between material constants and strain and can be written as follows:

$$\begin{cases}\beta=B_0+B_1\varepsilon+B_2\varepsilon^2+B_3\varepsilon^3+B_4\varepsilon^4+B_5\varepsilon^5\\ \alpha=A_0+A_1\varepsilon+A_2\varepsilon^2+A_3\varepsilon^3+A_4\varepsilon^4+A_5\varepsilon^5\\ n=N_0+N_1\varepsilon+N_2\varepsilon^2+N_3\varepsilon^3+N_4\varepsilon^4+N_5\varepsilon^5\\ Q=E_0+E_1\varepsilon+E_2\varepsilon^2+E_3\varepsilon^3+E_4\varepsilon^4+E_5\varepsilon^5\\ \ln A=D_0+D_1\varepsilon+D_2\varepsilon^2+D_3\varepsilon^3+D_4\varepsilon^4+D_5\varepsilon^5\end{cases} \tag{25}$$

As can be seen in Fig. 15, material constants have opposite behavior for two used metals, so material constants such as β, α, and n for aluminum increase with increasing strains, but the opposite occurs for copper. While with increasing strain, the values of Q and $\ln A$ increase for copper and decrease for AA7022 alloy. As shown in Fig. 15, raising the values of Q with strain for copper indicates the dominance of the work hardening mechanisms (dislocation mechanism), which is shown for the hot flow behavior of copper in Fig.10. But for aluminum, the decrease in activation energy with increasing strain indicates that deformation becomes easier and softening mechanism like DRV is dominant. The prime explanation is the activation of cross-slip and dislocation climb mechanisms at high deformation [55]. Table 6 and Table 7 illustrate the material constants for AA7022 aluminum alloy and pure copper, respectively.

The FS of the Al/Cu bimetal composite can be modeled by obtaining coefficients and material constants of developed constitutive equations to describe the flow stress behavior of aluminum and copper. Therefore, the effects of the strain are not considered in Eqs. (5)−(9) and this reduces the efficiency and accuracy of modeling the behavior of the Al/Cu composite. In this regard, the material parameters in a fifth-order strain-compensated constitutive model for the Al/Cu composite can be obtained according to Eqs. (26)−(30) by extending the obtained coefficients of the Arrhenius equation of aluminum and copper and applying the effect of strain in Eqs. (5)−(9). And finally, the FS behaviors of the Al/Cu bimetal composites are modeled by placing them in Eqs. (3) and (4). Another way to obtain the FS of the Al/Cu composite is by placing the stress and volume fraction of each constituent (aluminum and copper) in Eq. (2), and finally, the flow behavior of this bimetal composite is modeled.

$$\ln A_{\mathrm{CCA}}=\left(\sum_{i=0}^{5}a_i\varepsilon^i\right)_{\mathrm{Al}}V_{\mathrm{Al}}+\left(\sum_{i=0}^{5}a_i\varepsilon^i\right)_{\mathrm{Cu}}V_{\mathrm{Cu}} \tag{26}$$

$$\beta_{\mathrm{CCA}}=\left(\sum_{i=0}^{5}B\varepsilon^i\right)_{\mathrm{Al}}V_{\mathrm{Al}}+\left(\sum_{i=0}^{5}B_i\varepsilon^i\right)_{\mathrm{Cu}}V_{\mathrm{Cu}} \tag{27}$$

$$n_{\mathrm{CCA}}=\left(\sum_{i=0}^{5}N_i\varepsilon^i\right)_{\mathrm{Al}}V_{\mathrm{Al}}+\left(\sum_{i=0}^{5}N_i\varepsilon^i\right)_{\mathrm{Cu}}V_{\mathrm{Cu}} \tag{28}$$

$$\alpha_{\mathrm{CCA}}=\left(\sum_{i=0}^{5}A_i\varepsilon^i\right)_{\mathrm{Al}}V_{\mathrm{Al}}+\left(\sum_{i=0}^{5}A_i\varepsilon^i\right)_{\mathrm{Cu}}V_{\mathrm{Cu}} \tag{29}$$

$$Q_{\mathrm{CCA}}=\left(\sum_{i=0}^{5}E_i\varepsilon^i\right)_{\mathrm{Al}}V_{\mathrm{Al}}+\left(\sum_{i=0}^{5}E_i\varepsilon^i\right)_{\mathrm{Cu}}V_{\mathrm{Cu}} \tag{30}$$

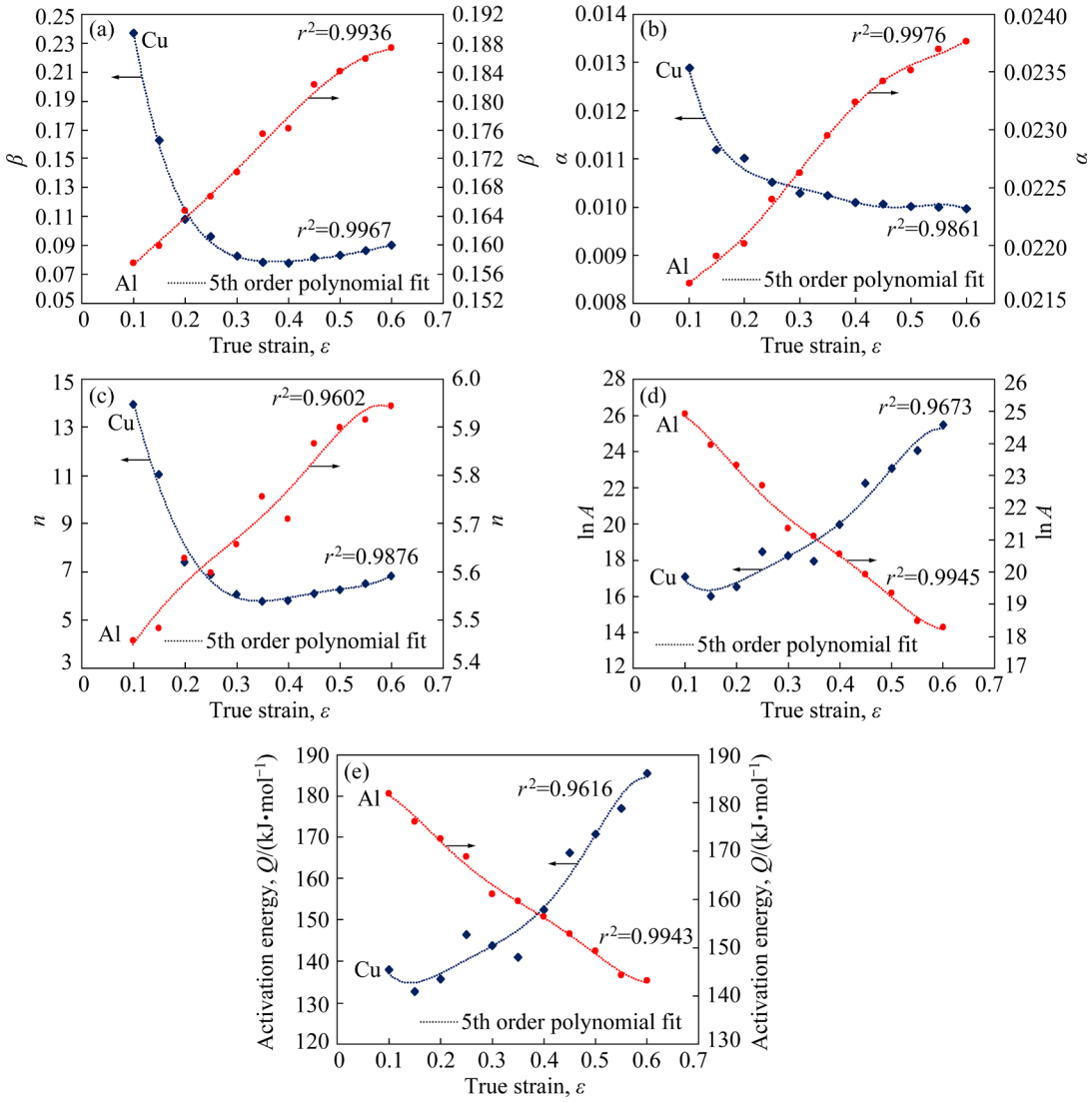

Fig. 15 Relationship between Q, n, β, ln A and α and true strain (ε) for AA7022 alloy and copper

Table 6 Fitting coefficients of polynomial curve for AA7022 alloy

β		α		n		Q		ln A	
B_0	0.1488	A_0	0.0212	N_0	5.2924	E_0	1.75×10^5	D_0	23.86
B_1	0.1116	A_1	0.008	N_1	1.4527	E_1	2.46×10^5	D_1	41.01
B_2	−0.3668	A_2	−0.0524	N_2	3.8959	E_2	-3×10^6	D_2	−439.63
B_3	1.2178	A_3	0.2575	N_3	−34.256	E_3	9×10^6	D_3	1506
B_4	−1.6257	A_4	−0.4868	N_4	82.643	E_4	-1×10^4	D_4	−2325.5
B_5	0.6570	A_5	0.3097	N_5	−63.507	E_5	8×10^6	D_5	1337.1

Table 7 Fitting coefficients of polynomial curve for copper

β		α		n		Q		ln A	
B_0	−17.72	A_0	−1.673	N_0	1396	E_0	-2.27×10^7	D_0	−3967
B_1	43.03	A_1	3.219	N_1	−2131	E_1	3.80×10^7	D_1	6803
B_2	−41.78	A_2	−2.395	N_2	947.4	E_2	-2.395×10^7	D_2	−4431
B_3	20.45	A_3	0.8663	N_3	28.95	E_3	7.238×10^6	D_3	1396
B_4	−5.031	A_4	−0.1559	N_4	−107	E_4	-9.95×10^5	D_4	−199.9
B_5	0.5739	A_5	0.02186	N_5	23.74	E_5	1.847×10^5	D_5	26.73

4.4 Developed constitutive equations verification

The material coefficients of the Arrhenius constitutive equation are extracted. Then the prediction of FS of Al/Cu bimetal composites based on the ROM method is established, considering various processing factors like temperatures, true strains, strain rates, and FSs of Al and Cu. To investigate validation of proposed equations, Figs. 16−18 illustrate the comparison among the flow stress obtained from experimental results and that predicted by the ROM method and the related equations in different volume fractions of elements. As is clear from these figures, the FS values predicated by ROM have good results and could be molding the experimental results of FS of Al/Cu bimetal composite at diverse processing states. In order to investigate the validation of the ROM model, average absolute relative error (AARE), root mean square error (RMSE), and correlation coefficient (R) that are considered as the statistical parameters were applied to showing the accuracy and their reliability. R is considered as a parameter that indicates the linear relationship of predicted values and available experimental data of FS and can be written as

$$r=\frac{\sum_{i=1}^{N}(E_i-\bar{E})(P_i-\bar{P})}{\sqrt{\sum_{i=1}^{N}(E_i-\bar{E})^2\sum_{i=1}^{N}(P_i-\bar{P})^2}} \tag{31}$$

$$\mathrm{AARE}=(\frac{1}{N})\sum_{i=0}^{N}\left|\frac{E_i-P_i}{E_i}\right|\times 100\% \tag{32}$$

$$\mathrm{RMSE}=\sqrt{\frac{1}{N}\sum_{i=0}^{N}(E_i-P_i)^2} \tag{33}$$

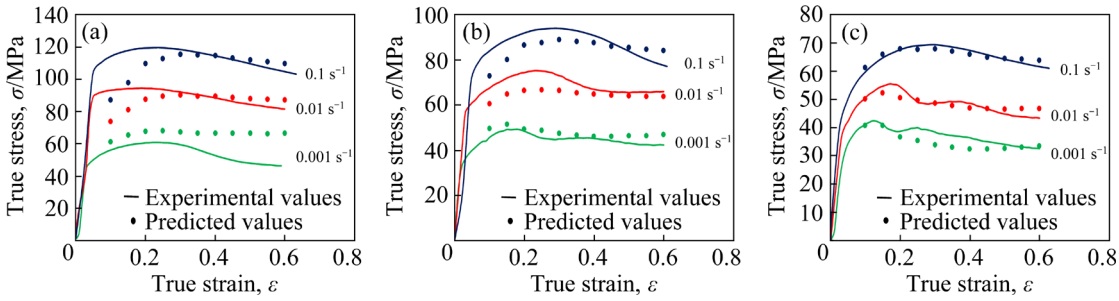

Fig. 16 Comparison between experimental and predicted FSs of Al/Cu composite with 51% Al at temperatures of 400 °C (a), 450 °C (b), and 500 °C (c)

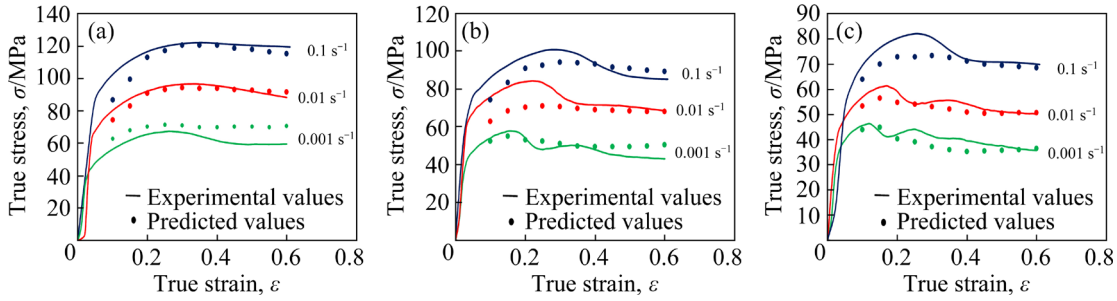

Fig. 17 Comparison between experimental and predicted FSs of Al/Cu composite with 42% Al at temperatures of 400 °C (a), 450 °C (b), and 500 °C (c)

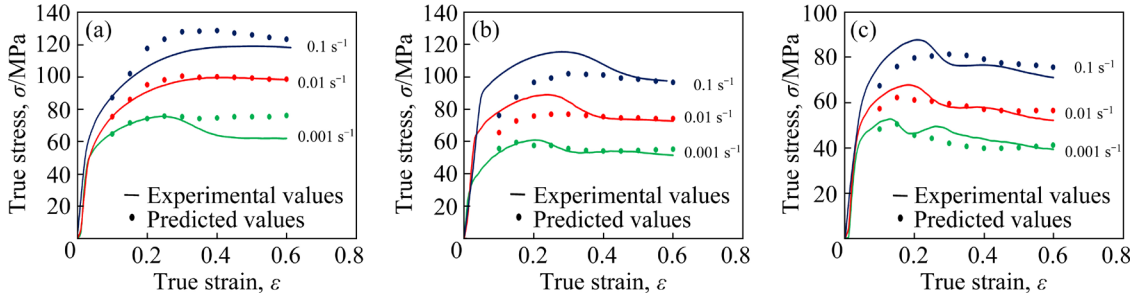

Fig. 18 Experimental and predicted FSs of Al/Cu composite with 30% Al at temperatures of 400 °C (a), 450 °C (b), and 500 °C (c)

where P_i and E_i are the experimental data and predicted results from ROM, respectively; N stands for the overall number of data; $\overline{E}$ and $\overline{P}$ are the average values of experimental and predicted results, respectively.

Figure 19 shows the correlations (R) among predicted results of FS from ROM and experimental FS data over the inter range of the processing parameter. The accuracy of the graph is indicated by a 45° line and the closer values to this line indicate better accuracy and performance of the output results. The analyses showed that the R values for the developed Arrhenius-type constitutive equation and ROM model were 0.9826, 0.9742 and 0.9718 for 51%, 42% and 30% Al, respectively. The AAREs for the proposed Arrhenius model by ROM model are 7.29, 6.31 and 5.97 for 51%, 42% and 30% Al, respectively. Also, the RSME values are calculated as 6.87, 5.58 and 6.92 MPa for 30%, 42% and 51% Al, respectively. Eventually, the average relative error variation for the developed model with 51%, 42% and 30% Al are 0.18%, 1.69% and −0.84%, respectively, as shown in Fig. 20.

Finally, based on Eqs. (26)−(30), the coefficients of the Arrhenius equation were predicted using a ROM model at a strain of 0.6 and compared with experimental data (the Arrhenius coefficients were calculated for CCA composite with different volume fractions of each component) which are presented in Table 8. The difference between experimental and predicted values proved the success of the ROM model to estimate the flow behavior of Al/Cu bimetal composites. The small error between the results can be related to the error of the Arrhenius equation of each material which many researchers have reported for different materials, and this error is negligible. Consequently, the obtained results prove that developed constitutive equations have sufficient accuracy and reliability to model the flow behavior of Al/Cu composite with increasing temperature.

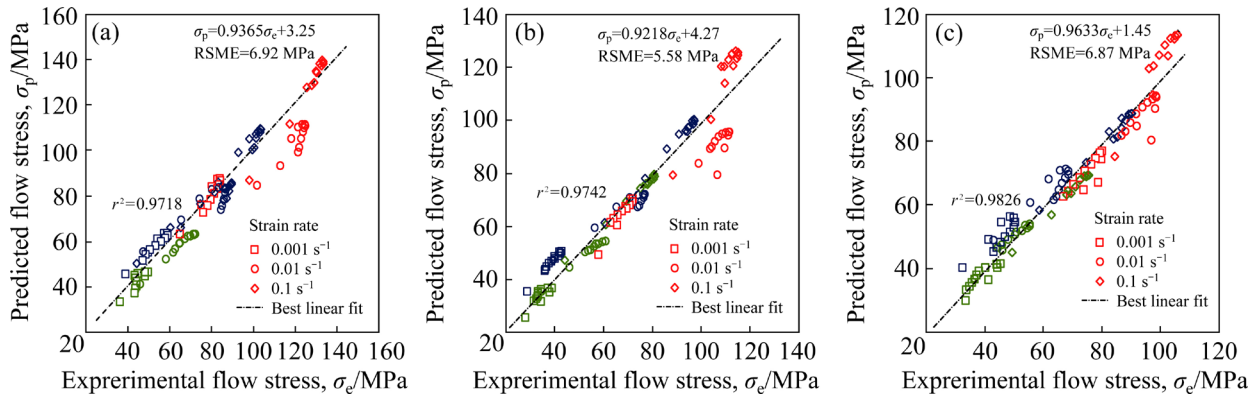

Fig. 19 Correlation between predicted results and experimental data of FS for Al/Cu composite with 30% Al (a), 42% Al (b), and 51% Al (c)

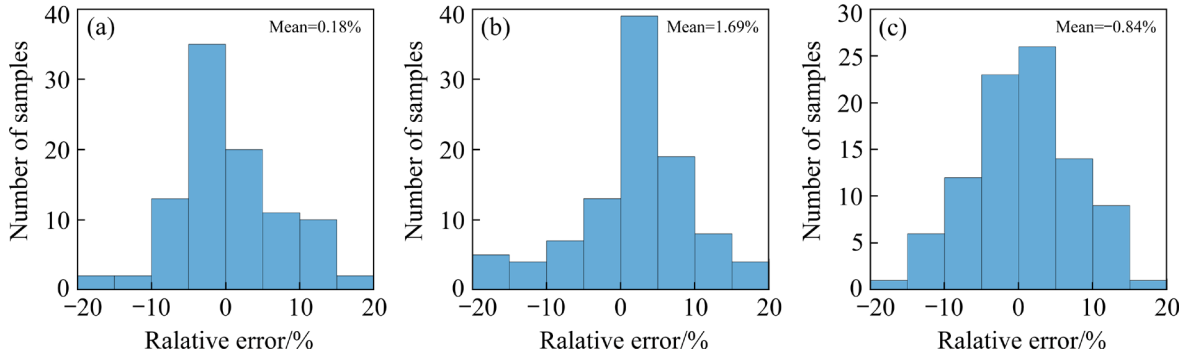

Fig. 20 Relative error between predicted results and experimental data of FS for Al/Cu composite with 30% Al (a), 42% Al (b), and 51% (c) Al

Table 8 Error between experimental data and ROM model predicated Arrhenius coefficients at strain of 0.6

Constant	Al	Cu	ROM			Experimental			Error/%
			51% Al	42% Al	30% Al	51% Al	42% Al	30% Al	
β	0.187	0.090	0.14	0.131	0.119	0.124	0.116	0.109	11.35
α	0.023	0.009	0.017	0.015	0.014	0.016	0.015	0.013	2.25
n	5.945	6.831	6.37	6.45	6.56	5.96	6.12	6.24	4.66
Q/(kJ·mol^{-1})	143	185	163	167	172	152	160	171	4.02
ln A	18.28	25.45	21.77	22.42	23.28	19.94	21.33	23.18	4.57

5 Conclusions

(1) The processing factors such as volume fraction of participating metals, forming temperature, strain rate, and strain have a significant effect on the hot flow behavior of the CCA composites as the FS decreases with increasing temperature and decreasing the strain rate. Also, the strength of composite samples increased by increasing the Cu component's volume fraction.

(2) The microstructure of hot deformed samples showed that the mechanism of deformed microstructure changes from DRV to DRX with increasing volume fraction of Cu component, and can be said that more nucleation of recrystallization occurs on these components by increasing the volume fraction of each constituent. Also, DRV is a dominant mechanism at low deformation temperature, whereas at high temperature, firstly, DRX occurs, and after that, grain growth occurs.

(3) A combination model of Arrhenius constitutive equation and strain-compensated Arrhenius constitutive equation with ROM model was developed to model the FS of Al/Cu composite with different processing parameters and volume fractions. The results showed good consistency between predicted results and experimental data.

References

[1] KHOSRAVIFARD A, EBRAHIMI R. Investigation of parameters affecting interface strength in Al/Cu clad bimetal rod extrusion process [J]. Materials & Design, 2010, 31(1):493−499. Doi: 10.1016/j.matdes.2009.06.026

[2] LEE W B, BANG K S, JUNG S B. Effects of intermetallic compound on the electrical and mechanical properties of friction welded Cu/Al bimetallic joints during annealing [J]. Journal of Alloys and Compounds, 2005, 390(1/2): 212−219. Doi: 10.1016/j.jallcom.2004.07.057

[3] LI Xiao-bing, ZU Guo-yin, WANG Ping. Effect of strain rate on tensile performance of Al/Cu/Al laminated composites produced by asymmetrical roll bonding [J]. Materials Science and Engineering A, 2013, 575: 61−64. Doi: 10.1016/j.msea.2013.03.056

[4] SHENG L Y, YANG F, XI T F, LAI C, YE H Q. Influence of heat treatment on interface of Cu/Al bimetal composite fabricated by cold rolling [J]. Composites Part B: Engineering, 2011, 42(6): 1468−1473. Doi: 10.1016/j.compositesb.2011.04.045

[5] SU Ya-jun, LIU Xin-hua, WU Yong-fu, HUANG Hai-you, XIE Jian-xin. Numerical simulation of temperature field in horizontal core-filling continuous casting for copper cladding aluminum rods [J]. International Journal of Minerals, Metallurgy and Materials, 2013, 20(7): 684−692. Doi: 10.1007/s12613-013-0784-6

[6] SAPANATHAN T, KHODDAM S, ZAHIRI S H, ZAREI-HANZAKI A. Strength changes and bonded interface investigations in a spiral extruded aluminum/copper composite [J]. Materials & Design, 2014, 57: 306−314. Doi: 10.1016/j.matdes.2014.01.030

[7] SHAYANPOOR A A, REZAEI ASHTIANI H R. Microstructural and mechanical investigations of powder reinforced interface layer of hot extruded Al/Cu bimetallic composite rods [J]. Journal of Manufacturing Processes, 2022, 77: 313−328. Doi: 10.1016/j.jmapro.2022.03.017

[8] HOSEINI ATHAR M M, TOLAMINEJAD B. Weldability window and the effect of interface morphology on the properties of Al/Cu/Al laminated composites fabricated by explosive welding [J]. Materials & Design, 2015, 86: 516−525. Doi: 10.1016/j.matdes.2015.07.114

[9] REZAEI ASHTIANI H R, SHAYANPOOR A A. New constitutive equation utilizing grain size for modeling of hot deformation behavior of AA1070 aluminum [J]. Transactions of Nonferrous Metals Society of China, 2021, 31(2): 345−357. Doi: 10.1016/S1003- 6326(21)65500-0

[10] REZAEI ASHTIANI H R, PARSA M H, BISADI H. Constitutive equations for elevated temperature flow behavior of commercial purity aluminum [J]. Materials Science and Engineering A, 2012, 545: 61−67. Doi: 10.1016/j.msea.2012.02.090

[11] YANG Qiu-mei, LIN Yong-cheng, GUO Jian-zheng, WANG Chao, CHEN Zi-jian, CHEN Kai-ge, ZHU

Jun-cheng. Spheroidization and dynamic recrystallization mechanisms of a novel HIPed P/M superalloy during hot deformation [J]. Journal of Alloys and Compounds, 2022, 910: 164909. Doi: 10.1016/j.jallcom.2022.164909

[12] LIU Shu-hui, PAN Qing-lin, LI Hang, HUANG Zhi-qi, LI Kuo, HE Xin, LI Xin-yu. Characterization of hot deformation behavior and constitutive modeling of Al−Mg−Si−Mn−Cr alloy [J]. Journal of Materials Science, 2019, 54(5): 4366–4383. Doi: 10.1007/s10853-018-3116-4

[13] MCQUEEN H J, RYAN N D. Constitutive analysis in hot working [J]. Materials Science and Engineering A, 2002, 322(1/2): 43−63. Doi: 10.1016/S0921-5093(01)01117-0

[14] JOHNSON G R, COOK W H. A constitutive model and data for metals subjected to large strains, high strain rates and high [C]//Proceedings of the 7th International Symposium on Ballistics. Hague, Netherlands, 1983: 541−547.

[15] HUANG Su-qing, KHAN A S. Modeling the mechanical behaviour of 1100-0 aluminum at different strain rates by the bodner-partom model [J]. International Journal of Plasticity, 1992, 8(5): 501−517. Doi: 10.1016/0749-6419(92)90028-B.

[16] SLOOFF F A, ZHOU J, DUSZCZYK J, KATGERMAN L. Constitutive analysis of wrought magnesium alloy Mg−Al4−Zn1 [J]. Scripta Materialia, 2007, 57(8): 759−762. Doi: 10.1016/j.scriptamat.2007.06.023

[17] CHEN Xiao-xue, ZHAO Guo-qun, ZHAO Xing-ting, WANG Yong-xiao, XU Xiao, ZHANG Cun-sheng. Constitutive modeling and microstructure characterization of 2196 Al−Li alloy in various hot deformation conditions [J]. Journal of Manufacturing Processes, 2020, 59: 326−342. Doi: 10.1016/j.jmapro.2020.09.063

[18] REZAEI ASHTIANI H R, SHAYANPOOR A A. Prediction of thermo-mechanical behavior and microstructural evolution of copper considering initial grain size at elevated temperature [J]. Materials Today Communications, 2021, 28: 102652. Doi: 10.1016/j.mtcomm.2021.102652

[19] LONG Jin-chuan, XIA Qin-xiang, XIAO Gang-feng, QIN Yi, YUAN Shuai. Flow characterization of magnesium alloy ZK61 during hot deformation with improved constitutive equations and using activation energy maps [J]. International Journal of Mechanical Sciences, 2021, 191:106069. Doi: 10.1016/j.ijmecsci.2020.106069

[20] SU Gang, YUN Zhong, LIN Yong-cheng, HE Dao-guang, ZHANG Song, CHEN Zi-jian. Microstructure evolution and a unified constitutive model of Ti-55511 alloy compressed at stepped strain rates [J]. Materials, 2021, 14(22): 6750. Doi: 10.3390/ma14226750

[21] ZHOU L, CUI C, WANG Q Z, LI C, XIAO B L, MA Z Y. Constitutive equation and model validation for a 31 vol.% B_4C_p/6061Al composite during hot compression [J]. Journal of Materials Science and Technology, 2018, 34(10): 1730−1738. Doi: 10.1016/j.jmst.2018.02.001

[22] KIM H S. On the rule of mixtures for the hardness of particle reinforced composites [J]. Materials Science and Engineering A, 2000, 289(1/2): 30−33. Doi: 10.1016/S0921-5093(00)00909-6

[23] PARAMSOTHY M, GUPTA M, SRIKANTH N. Processing, microstructure, and properties of a Mg/Al bimetal macrocomposite [J]. Journal of Composite Materials, 2008, 42(24): 2567−2584. Doi: 10.1177/0021998308098369

[24] HAWKINS R, WRIGHT J C. Observations on the deformation properties of sandwich materials [J]. International Journal of Mechanical Sciences, 1972, 14(12): 875−878. Doi: 10.1016/0020-7403(72)90046-X

[25] FENG Bo, XIN Yun-chang, GUO Fei-long, YU Hui-hui, WU Yang, LIU Qing. Compressive mechanical behavior of Al/Mg composite rods with different types of Al sleeve [J]. Acta Materialia, 2016, 120: 379−390. Doi: 10.1016/j.actamat.2016.08.079

[26] KANG C G, JUNG Y J, KWON H C. Finite element simulation of die design for hot extrusion process of Al/Cu clad composite and its experimental investigation [J]. Journal of Materials Processing Technology, 2002, 124(1/2): 49−56. Doi: 10.1016/S0924-0136(02)00106-1

[27] LUO Jun-ting, ZHAO Shuang-jing, ZHANG Chun-xiang. Microstructure of aluminum/copper clad composite fabricated by casting-cold extrusion forming [J]. Journal of Central South University of Technology (English Edition), 2011, 18(4): 1013−1017. Doi: 10.1007/s11771-011-0796-1

[28] SAPANATHAN T, KHODDAM S, ZAHIRI S H. Spiral extrusion of aluminum/copper composite for future manufacturing of hybrid rods: A study of bond strength and interfacial characteristics [J]. Journal of Alloys and Compounds, 2013, 571: 85−92. Doi: 10.1016/j.jallcom.2013.03.210

[29] LIN Y C, ZHAO Chun-yang, CHEN Ming-song, CHEN Dong-dong. A novel constitutive model for hot deformation behaviors of Ti−6Al−4V alloy based on probabilistic method [J]. Applied Physics A: Materials Science and Processing, 2016, 122(8): 716. Doi: 10.1007/s00339-016-0248-8

[30] VERLINDEN B, DRIVER J, SAMAJDAR I, Doherty R. Thermo-mechanical processing of metallic materials [M]. 1nd ed. Amsterdam: Elsevier, 2007.

[31] LIN Y C, WU Xian-yang, CHEN Xiao-min, CHEN Jian, WEN Dong-xu, ZHANG Jin-long, LI Lei-ting. EBSD study of a hot deformed nickel-based superalloy [J]. Journal of Alloys and Compounds, 2015, 640: 101−113. Doi: 10.1016/j.jallcom.2015.04.008

[32] HUMPHREYS F J, HATHERLY M, ROLLETT A, ROHRER G. Control of recrystallization [M]//Recrystallization and Related Annealing Phenomena. Amsterdam: Elsevier, 2004: 469−505.

[33] SAMANTARAY D, MANDAL S, PHANIRAJ C, BHADURI A K. Flow behavior and microstructural evolution during hot deformation of AISI Type 316 L(N) austenitic stainless steel [J]. Materials Science and Engineering A, 2011, 528(29/30): 8565−8572. Doi: 10.1016/j.msea.2011.08.012

[34] HAN Ying, QIAO Guan-jun, SUN Jia-peng, ZOU De-ning. A comparative study on constitutive relationship of as-cast 904L austenitic stainless steel during hot deformation based on Arrhenius-type and artificial neural network models [J]. Computational Materials Science, 2013, 67: 93−103. Doi:

10.1016/j.commatsci.2012.07.028

[35] ASHTANI REZAI H R, SHAHSAVARI P. Constitutive modeling of flow behavior of precipitation-hardened AA7022-T6 aluminum alloy at elevated temperature [J]. Transactions of Nonferrous Metals Society of China, 2020, 30(11): 2927−2940. Doi: 10.1016/S1003- 6326(20)65432-2

[36] SHI Cang-ji, MAO Wei-min, CHEN X G. Evolution of activation energy during hot deformation of AA7150 aluminum alloy [J]. Materials Science and Engineering A, 2013, 571: 83−91. Doi: 10.1016/j.msea.2013.01.080

[37] ZHANG Hong-bin, ZHANG Kai-feng, JIANG Shao-song, ZHOU Hai-ping, ZHAO Chang-hong, YANG Xiao-li. Dynamic recrystallization behavior of a γ'-hardened nickel-based superalloy during hot deformation [J]. Journal of Alloys and Compounds, 2015, 623: 374−385. Doi: 10.1016/j.jallcom.2014.11.056

[38] SUN Yu, CAO Zhuo-han, WAN Zhi-peng, HU Lian-xi, YE Wen-hong, LI Nian-kui, FAN Chang-long. 3D processing map and hot deformation behavior of 6A02 aluminum alloy [J]. Journal of Alloys and Compounds, 2018, 742: 356−368. Doi: 10.1016/j.jallcom.2018.01.299

[39] YIN Hao, LI Hong-ying, SU Xiong-jie, HUANG De-sheng. Processing maps and microstructural evolution of isothermal compressed Al−Cu−Li alloy [J]. Materials Science and Engineering A, 2013, 586: 115−122. Doi: 10.1016/j.msea.2013.07.084

[40] LIU Ying, XIONG Wei, YANG Qing, ZENG Ji-wei, ZHU Wen, SUNKULP G. Constitutive behavior and processing map of T2 pure copper deformed from 293 to 1073 K [J]. Journal of Materials Engineering and Performance, 2018, 27(4): 1812−1824. Doi: 10.1007/s11665-018-3210-4

[41] NNAMCHI P, YOUNES A, GONZÁLEZ S. A review on shape memory metallic alloys and their critical stress for twinning [J]. Intermetallics, 2019, 105: 61−78. Doi: 10.1016/j.intermet.2018.11.005.

[42] MIRZADEH H, CABRERA J M, NAJAFIZADEH A, CALVILLO P R. EBSD study of a hot deformed austenitic stainless steel [J]. Materials Science and Engineering A, 2012, 538: 236−245. Doi: 10.1016/j.msea.2012.01.037

[43] MOHAMADIZADEH A, ZAREI-HANZAKI A, ABEDI H R. Modified constitutive analysis and activation energy evolution of a low-density steel considering the effects of deformation parameters [J]. Mechanics of Materials, 2016, 95: 60−70. Doi: 10.1016/j.mechmat.2016.01.001

[44] REZAEI ASHTIANI H R, SHAYANPOOR A A. Effect of initial grain size on the hot deformation behavior and microstructural evolution of pure copper [J]. Acta Metallurgica Sinica (English Letters), 2021, 35(4): 662−678. Doi: 10.1007/s40195-021-01346-7

[45] HE Wen-xiong, WANG Er-de, HU Lian-xi, YU Yang, SUN Hong-fei. Effect of extrusion on microstructure and properties of a submicron crystalline Cu−5wt.%Cr alloy [J]. Journal of Materials Processing Technology, 2008, 208(1/2/3): 205−210. Doi: 10.1016/j.jmatprotec.2007.12.107

[46] MOSTAFAEI M A, KAZEMINEZHAD M. Hot deformation behavior of hot extruded Al−6Mg alloy [J]. Materials Science and Engineering A, 2012, 535: 216−221. Doi: 10.1016/j.msea.2011.12.067

[47] ZHANG R F, GERMANN T C, WANG J, LIU X Y, BEYERLEIN I J. Role of interface structure on the plastic response of Cu/Nb nanolaminates under shock compression: Non-equilibrium molecular dynamics simulations [J]. Scripta Materialia, 2013, 68(2): 114−117. Doi: 10.1016/j.scriptamat.2012.09.022

[48] PARAMSOTHY M, GUPTA M, SRIKANTH N. Improving compressive failure strain and work of fracture of magnesium by integrating it with millimeter length scale aluminum [J]. Journal of Composite Materials, 2008, 42(13): 1297−1307. Doi: 10.1177/0021998308092198

[49] YANG Yong-biao, ZHANG Zhi-min, LI Xu-bin, WANG Qiang, ZHANG Yan-hui. The effects of grain size on the hot deformation and processing map for 7075 aluminum alloy [J]. Materials & Design, 2013, 51: 592−597. Doi: 10.1016/j.matdes.2013.04.034

[50] YANG J Y, KIM W J. The effect of addition of Sn to copper on hot compressive deformation mechanisms, microstructural evolution and processing maps [J]. Journal of Materials Research and Technology, 2020, 9(1): 749−761. Doi: 10.1016/j.jmrt.2019.11.015

[51] LI Ning, ZHAO Cheng-zhi, JIANG Zhu-hang, ZHANG He-xin. Flow behavior and processing maps of high-strength low-alloy steel during hot compression [J]. Materials Characterization, 2019, 153: 224−233. Doi: 10.1016/j.matchar.2019.05.009

[52] ZHANG Jing-qi, DI Hong-shuang, WANG Hong-tao, MAO Kun, MA Tian-jun, CAO Yu. Hot deformation behavior of Ti-15-3 titanium alloy: A study using processing maps, activation energy map, and Zener−Hollomon parameter map [J]. Journal of Materials Science, 2012, 47(9): 4000−4011. Doi: 10.1007/s10853-012-6253-1

[53] MIRZADEH H. Simple physically-based constitutive equations for hot deformation of 2024 and 7075 aluminum alloys [J]. Transactions of Nonferrous Metals Society of China, 2015, 25(5): 1614−1618. Doi: 10.1016/S1003-6326(15)63765-7

[54] WANG Hao-ran, ZHANG Zhi-yuan, ZHAI Rui-xue, MA Rui, ZHAO Jun. New method to develop high temperature constitutive model of metal based on the Arrhenius-type model [J]. Materials Today Communications, 2020, 24: 101000. Doi: 10.1016/j.mtcomm.2020.101000

[55] SHEPPARD T, NORLEY J. Deformation characteristics of Ti−6Al−4V [J]. Materials Science and Technology (United Kingdom), 1988, 4(10): 903−908. Doi: 10.1179/mst.1988.4.10.903

不同成分铝/铜双金属复合材料的热变形行为及其本构模型

Amir Arsalan SHAYANPOOR, Hamid Reza REZAEI ASHTIANI

School of Mechanical Engineering, Arak University of Technology, Arak, Iran

摘　要：通过等温压缩实验，研究 Al/Cu 双金属复合材料在 400~500 ℃、应变速率 0.001~0.1 s^{-1} 条件下的热变形行为，并考虑复合材料成分体积分数(Al 含量为 30%~51%)的影响。采用 Arrhenius 模型和混合定律(ROM)模型建立新的本构方程。流变应力(FS) 实验表明，工艺参数和体积分数对复合材料的流变行为有影响，而 Cu 的体积分数对复合材料的高温流变行为影响更大。对于体积分数为 51%、42%和 30% Al 的复合材料，建立的 Arrhenius 型本构方程和 ROM 模型的相关系数(R)分别为 0.9826、0.9742 和 0.9718，其平均相对误差分别为 0.18%、1.69%和−0.84%。结果表明，新建立的本构模型能较好地预测双金属复合材料的热加工行为。最后，研究不同工艺条件下复合材料的显微组织，确定三种不同成分 Al/Cu 复合材料在不同温度、应变和应变速率范围内的主要热变形机制。

关键词：铝/铜双金属复合材料；热变形；混合定律(ROM)；本构方程；力学行为；显微组织

(Edited by Xiang-qun LI)